

Characterization of DNA conformation inside bacterial viruses

Anton S. Petrov, C. Rebecca Locker, and Stephen C. Harvey*

School of Biology, Georgia Institute of Technology, 310 Ferst Dr., Atlanta, Georgia 30332, USA

(Received 13 April 2009; published 14 August 2009)

In this study we develop a formalism to describe the organization of DNA inside bacteriophage capsids during genome packaging. We have previously shown that DNA inside bacteriophage phi29 (ϕ 29) is organized into folded toroids [A. S. Petrov and S. C. Harvey, *Structure* **15**, 21 (2007)], whereas epsilon15 (ϵ 15) reveals the coaxial organization of the genetic material [A. S. Petrov, K. Lim-Hing, and S. C. Harvey, *Structure* **15**, 807 (2007)]. We now show that each system undergoes two consecutive transitions. The first transition corresponds to the formation of global conformations and is analogous to a disorder-order conformational transition. The second transition is characterized by a significant loss of DNA mobility at the local level leading to glasslike dynamic behavior. Packing genetic material inside bacteriophages can be used as a general model to study the behavior of semiflexible chains inside confined spaces, and the proposed formalism developed here can be used to study other systems of linear polymer chains confined to closed spaces.

DOI: [10.1103/PhysRevE.80.021914](https://doi.org/10.1103/PhysRevE.80.021914)

PACS number(s): 87.15.A-, 82.35.Pq, 82.39.Pj, 87.15.N-

I. INTRODUCTION

Bacteriophages (or bacteriophages) are a subclass of viruses that infect bacteria. They consist of a preassembled outer protein shell (capsid) enclosing viral genetic material (DNA or RNA) that is deposited into cells by adenosine triphosphate (ATP)-driven molecular motors [1]. DNA organization inside bacteriophages has received growing experimental attention in the past few years [2]. The average DNA conformations inside capsids were visualized by generating three-dimensional (3D) reconstructions of cryoelectron microscopy images [3,4]. There have also been a number of computational studies that simulate the injection process of the DNA chain inside viral capsids represented by coarse-grained models [5–14]. Another group of studies [15–20] treated the confined DNA within the framework of continuum models and used statistical mechanics [21–23] to predict thermodynamic properties of DNA such as pressure, forces and free energy. However, the continuum approach required *a priori* knowledge of a DNA conformation inside the phages, which is often assumed to be an “inverse spool.” While this conformation may minimize the DNA enthalpy, it neglects the entropic effect of confinement [17].

DNA confinement in capsids is analogous to the polymer physics problem of confining a semiflexible polymer chain inside a cavity [24]. The confinement process of such class of polymers, which includes DNA, is characterized by a competition of the enthalpic and entropic components of the free energy. Both of these terms, in general, have a complex dependence on three characteristic lengths of the confined systems, which include the contour length of the polymer, its persistence length, and the linear dimensions of the cavity.

A theory of phase transitions for a system of semiflexible chains has been proposed by extending basic ideas of Onsager’s theory [25] for rigid rods. In particular, it has been shown [24,26] that the order parameter at the point of the

isotropic-nematic phase transition for a system of semiflexible rods reaches the value of 0.49, which is significantly lower than that for a system of rigid rods (0.84). However, this approach considers an ensemble of semiflexible chains instead of characterizing the behavior of a single chain, and it does not consider confinement to any particular geometry.

Early studies on polymers in confined geometries used the ideal chain approximation, wherein the interactions between non-neighboring monomers are neglected, to estimate the free energy change associated with confinement [27–29]. In general, these models are only valid when the confinement is weak [24,30]. If the chain is confined within a slit or within a cylinder, the concentration of monomers does not depend on the chain length. It has been shown by Casassa that for the cases of weak confinement the excess of the free energy is linearly proportional to the chain length N [27]. However, this is no longer true for a chain confined within a spherical cavity because the polymer volume fraction increases upon confinement making volume exclusion effects non-negligible. A blob scaling theory that describes the strong confinement regime, thus accounting for volume exclusion effects, has also been proposed for flexible chains [24,31]. The theory predicts that the free-energy scales as $N^{9/4}$, where N is the total number of monomers in the chain. It has also been shown that the same scaling laws apply for systems where multiple flexible chains are confined in spherical cavities in the dilute and semidilute regimes. This implies that the free energy of each individual chain scales independently from the other chains in the system [32]. The blob scaling theory has recently been extended to the case of semiflexible chains. Sakaue [33] proposed a phase diagram for a semiflexible chain of length N confined in a spherical cavity of size D . Several confinement regimes were identified. While some of these regimes depend on a particular chain flexibility mechanism, others were found to exist universally. When the concentration of the confined semiflexible chains is low (with the polymer volume fraction less than 0.2), properties are self-averaging and analogous to semidilute solutions. In that case, nonlinear scaling laws still hold. The same laws also describe the systems containing several DNA chains inside spherical cavity in the range of concentrations 0–0.2

*Corresponding author. FAX: +1 404 894 0519; steve.harvey@biology.gatech.edu

[32]. However, cases with high concentrations of a polymer inside the cavity were not considered. The latter cases do not have a universal description since their properties depend on the specific flexibility mechanism of the chains.

A number of simulation studies have predicted the dependence of some properties of ideal polymer chains confined inside a sphere, e.g., end-to-end distance [34]. The models revealed the dependence in the chain behavior on the diameter of the sphere and the chain flexibility. However, the behavior of real polymers is significantly different from that of ideal chains [35], particularly in the case of strong confinement where volume exclusion and other long-range interactions, e.g., electrostatics, have a higher impact on chain behavior. Another group [36] tested the effect of polycations on the structural and thermodynamic properties of polyelectrolytes confined to cavities and showed that the compaction of the systems increases with the valence of a polycation. Recent Monte Carlo simulations [37,38], which took into account the effect of excluded volume, revealed the limits of the ideal chain models, and, furthermore, proved the nonlinear power laws proposed by the strong confinement regime theories [33]. Molecular dynamics (MD) simulations of multiple flexible chains inside spheres corroborated the exponential laws predicted by the strong confinement theory [32]. Recently an analytical approach to describe the behavior of semiflexible wormlike chains has been developed [39]. Although it shows very good agreement with Langevin dynamics simulations, this approach omits from consideration excluded volume effects, which are essential in the case of viral DNA.

The packing of DNA (a semiflexible polymer with a Kuhn length of ~ 1000 Å) inside bacteriophage capsids (which typically range in size of 200–2000 Å) certainly corresponds to strong confinement in the bending regime [33]. It cannot be described by current theoretical models because the DNA has a high volume fraction within the capsid (0.4–0.6) and the strong bending regime. These factors lead to properties that are not self-averaging and quite sensitive to the shape and size of the bacteriophages. A first attempt to characterize the ordering of DNA inside bacteriophages has been recently performed by Marenduzzo [40]. We have recently simulated DNA packing inside bacteriophages phi29 ($\phi 29$) and epsilon15 ($\epsilon 15$) using a coarse-grained model and an extensive molecular dynamics protocol. The $\phi 29$ capsid is slightly elongated with the dimensions 420×540 Å modeled by extended pentakisidodecahedron [41], whereas that of $\epsilon 15$ is a regular icosahedron with a diameter of ~ 650 Å, which contains a large cylindrical protein portal complex located in the capsid's interior [42]. Our simulations revealed that DNA inside $\phi 29$ is predominantly organized into folded-toroidal conformations and a coaxial-spooling motif was observed inside $\epsilon 15$ (Fig. 1). Both conformations have also been predicted using the statistical approach [43], in which the polymer was treated as a line. The main factors that determine a conformation of DNA inside bacteriophages have been discussed in our previous publications [44,45]. In the current work we go beyond the simple visual characterization of DNA conformation and introduce several structural parameters to characterize the individual DNA conformations and dynamics of packaging inside closed confined

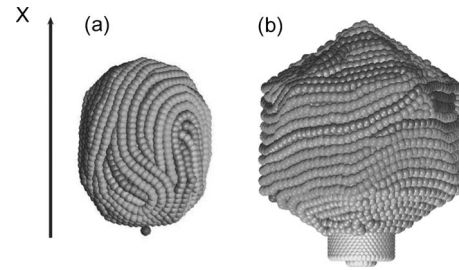


FIG. 1. Conformations of DNA inside bacteriophages (a) $\phi 29$ and (b) $\epsilon 15$ with respect to the external axis X , which corresponds to the direction of packaging.

spaces over a wide range of packing densities.

II. METHODS

A. Molecular dynamics simulations

The details of simulations are given elsewhere [12,41]. Here we only provide a brief summary. DNA packaging was simulated within the framework of a semiflexible coarse-grained model of beads on a string, with each bead representing 6 base pairs [41]. The capsids were modeled by polyhedrons described above, whose faces and edges were filled by a number of soft spheres with radius of 8.0 Å to prevent penetration of DNA through the capsid walls. The force field accounted for elastic stretching and bending by harmonic potentials, DNA-capsid interactions through a semiharmonic repulsion between the capsid walls made of closed packed spheres and DNA beads, and long-range electrostatic interactions between DNA molecules. The last term, which treats the solvent implicitly, is derived from the experimental data of Rau and Parsegian and modeled as a function of distance, r , by a Debye-Huckel-type function

$$E_{DNA-DNA}(r) = L_b \frac{q_{eff}^2 \exp[-\kappa_{eff}(r-2a)]}{r}, \quad (1)$$

where the effective charge, $q_{eff} = -12.6 e$ per pseudoatom, the effective screening constant, $\kappa_{eff} = 0.31 \text{ \AA}^{-1}$, $L_b = 7.135 \text{ \AA}$ (Bjerrum length), and DNA radius, $a = 12.5 \text{ \AA}$. All the other force field constants were derived to match the thermodynamic properties of DNA molecules. The DNA elastic parameters are chosen to match the known elastic moduli for stretching and bending; the former is computed from the average rise per base pair of free dsDNA reported in the nucleic acid database and the latter is derived from the experimentally observed persistence length of DNA (500 Å). Specifically, the numerical values of constants are $k_b = 3.5 \text{ kcal}/(\text{mol} \cdot \text{Å}^2)$, $b_0 = 19.9 \text{ \AA}$, $k_\theta = 22.4 \text{ kcal}/(\text{mol} \cdot \text{rad}^2)$, $\theta_0 = \pi \text{ rad}$, $k_{DNA-DNA} = 11.0 \text{ kcal}/(\text{mol} \cdot \text{Å}^2)$, $d_{0,DNA-DNA} = 25.0 \text{ \AA}$, $k_{DNA-Capsid} = 8.8 \text{ kcal}/(\text{mol} \cdot \text{Å}^2)$, $d_{0,DNA-Capsid} = 20.5 \text{ \AA}$. A cut-off distance of 50 Å was used for calculating the volume exclusion terms and that of 75 Å was used in the calculations of the long range DNA-DNA interactions. Thus, all parameters were obtained independently in any directly measured thermodynamic properties of bacteriophages. The genome of $\phi 29$ consists of 19 657 base pairs and was modeled by 3217

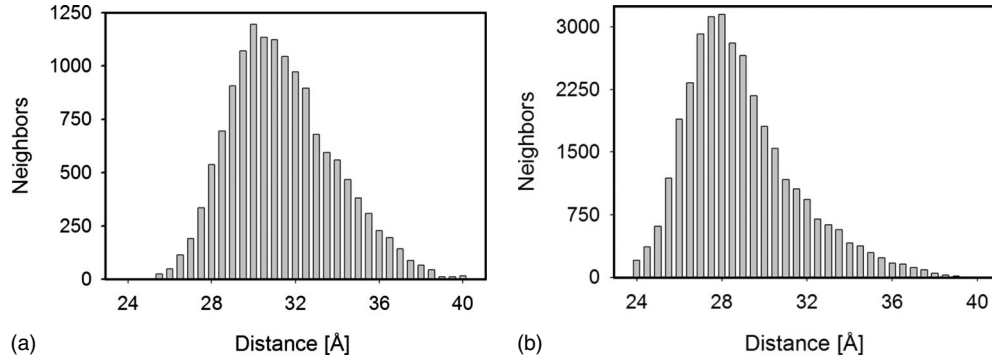


FIG. 2. Distribution of the nearest segments with respect to a given segment \mathbf{u}_i for fully packed bacteriophages (a) $\phi 29$ and (b) $\epsilon 15$. The cut-off distance of 42 Å was used to construct these histograms.

beads; the genome length and number of pseudoatoms used in the coarse grained representation of $\epsilon 15$ was 39 671 and 6601, respectively. Typical packaging conformations of $\phi 29$ and $\epsilon 15$ are shown in Fig. 1. Beads were injected inside bacteriophage in 10 Å increments (half a bead at a time), each of which was followed by extensive molecular dynamics equilibration.

All MD trajectories for packaging DNA inside bacteriophages were generated with a time step of 1 ps at 300K by coupling the systems to a Berendsen thermostat [46]. Simulations were performed within the framework of the coarse-grained model by using YUP, a freely available MD package [47]. During the packaging simulations, the motion of DNA was not restricted by anything but capsid walls, and no *a priori* conformation of DNA was assumed. The length of packing trajectories was 70 μ s and 230 μ s for $\phi 29$ and $\epsilon 15$, respectively. This is several orders of magnitude faster than the packaging time *in vivo* or *in vitro* but sufficient to maintain the equilibrium at every point along the trajectories since the model is coarse grained. The equilibrium of the systems was tested by monitoring the energy of the systems at every 10% of DNA packed. The results of these tests are reported in our previous publications [41]. Ten independent packing trajectories for each bacteriophage have been used for all ensemble-averaged properties presented in the current manuscript.

To collect equilibrium properties at a zero packaging rate, additional equilibrium trajectories of 500 ns were generated by starting MD simulations using initial conformations from the conformations saved at every ten percent packed along the initial packing trajectories. A total of 1000 data points have been collected from each equilibrium trajectory at 500 ps intervals. All quantities described here are presented as a function of the absolute packing density defined as volume (DNA)/volume (capsid); these values for the fully packed bacteriophages $\phi 29$ and $\epsilon 15$ are 0.46 and 0.52, respectively.

B. Calculation of the nematic order parameter

The order parameter that describes a transition from an isotropic to a nematic phase is often defined as the second Legendre polynomial $\langle P_2(\cos \theta) \rangle$, which can be computed as

$$S = \langle P_2(\cos \theta) \rangle = \frac{1}{N} \left\langle \sum \frac{1}{2} (3 \cos^2 \theta - 1) \right\rangle \quad (2)$$

where θ is an angle between the orientation of a particle and the nematic director vector. It varies from 0 to π ; the lower limit corresponds to a completely randomly oriented isotropic phase and the upper limit is reached when the system is completely aligned.

The definition of the nematic order parameter given by Eq. (2) assumes that the direction of the nematic director is known. However, an appropriate *a priori* choice of this director vector may be not always obvious. Because of that, a more general definition of the nematic order parameter proposed by Eppenga and Frenkel [48,49] will also be used in our analysis. It is defined as

$$S^2 = \frac{1}{N} \sum_{i=1}^N \langle \mathbf{n} \cdot \mathbf{Q}_i \cdot \mathbf{n} \rangle, \quad (3)$$

with

$$\mathbf{Q}_i = \sum_{j=1}^{N_{nn}^i} \left(\frac{3}{2} \mathbf{u}_j^i \mathbf{u}_j^i - \frac{1}{2} \mathbf{I} \right), \quad (4)$$

where N_{nn}^i is the number of the nearest neighbors for segment i (discussed below), \mathbf{u}_j^i is a DNA segment j from the nearest-neighbor list of segment i , and \mathbf{n} is an arbitrary unit vector. The nematic order parameter was obtained as the largest positive eigenvalue (λ_+) of the traceless second rank tensor given by Eq. (4). Thus, the director vector is internally defined by the orientation of the DNA segments independently in any external coordinate frame. The calculations of the nematic order parameter have been performed in both global and local ways. In the former case the tensors were constructed from all segments inside the capsids, and the calculated eigenvalues were averaged over ten different conformations. To obtain the local-order parameters, first, the tensor \mathbf{Q}_i was constructed for the set of nearest neighbors of a given segment \mathbf{u}_i defined as a vector connecting two consecutive beads. The nearest neighbors were determined by the following procedure. If for a given segment \mathbf{u}_i , there is a segment \mathbf{u}_j^i , which is not directly connected to \mathbf{u}_i and located within a cut-off distance of 38 Å (the distance that deter-

mines the first coordination shell in the radial distribution function calculated for $\phi 29$ and $\epsilon 15$ —Fig. 2), it has been added to the nearest-neighbor list of segment \mathbf{u}_i . If two or more directly bonded segments, which are nearest neighbors to \mathbf{u}_i (e.g., \mathbf{u}_j^i and \mathbf{u}_{j+1}^i), satisfy the cut-off criteria, only the closest segment is added to the list. The eigenvalues of the local tensors were evaluated for each segment \mathbf{u}_i . The results were averaged over all segments \mathbf{u}_i , and then averaged over ten different conformations.

C. Calculations of the bond-orientational parameter

The bond-orientational order parameter that describes presence of hexagonal phase inside capsids [50] was calculated according to the definition of Nelson and co-workers [51–53]

$$\Psi_6 = \frac{1}{6} \sum_{i=1}^N (e^{6i\theta}), \quad (5)$$

where θ is “bond angle,” which is defined as an angle between the lines that connect centers of the segment i and its nearest neighbors.

D. Calculation of the correlation function and average displacements

Correlation functions are calculated using data from the additional equilibrium trajectories. The conformations extracted every ten percent along the packaging trajectories are used as the starting points. The original orientation of every DNA segment $\mathbf{u}_i(0)$ inside the capsids is used as a reference orientation to calculate the projections of the instantaneous orientation of the segments $\mathbf{u}_i(t)$ and to evaluate the correlation function

$$g_{-2}(t) = \left\langle \frac{1}{2} \sum_i \{3 \cos^2[\mathbf{u}_i(0) \cdot \mathbf{u}_i(t)] - 1\} \right\rangle. \quad (6)$$

The relaxation time, τ_{sl} , for the correlation functions was obtained by fitting the values of $g_{-2}(t)$ into the double-exponential function with four free parameters.

$$g_{-2}(t) = g_{-2f} \exp(-\tau_f/t) + g_{-2sl} \exp(-\tau_{sl}/t). \quad (7)$$

This function describes two relaxation processes. The fast relaxation (denoted by subscript f), occurs at the beginning of every force trajectory and describes the initial relaxation (equilibration) of the system after its restart from a trajectory point with a new set of velocities drawn from the Boltzmann distribution. The slow relaxation (denoted by subscript sl), describes the approach of the correlation function to zero and represents a measure of the system’s mobility.

The displacements of all the DNA beads over 500 ps have been calculated by comparing their positions between each pair of the consecutive frames in the equilibrium trajectories. The results have been averaged over the number of frames and the number of beads.

III. RESULTS

A. Characterization of the DNA order inside the capsids

1. External order parameter

Visual analysis of packing trajectories allowed us to characterize the behavior of DNA into stages [41,42]. At the early stages of packaging, DNA inside bacteriophages is highly disordered and it moves through all available space but, because the dimensions of the bacteriophage capsids are comparable to DNA persistence length, it has a tendency to concentrate more near the capsid boundaries to minimize the bending stress [41,42]. When nearly half of genome is packed, DNA forms a global conformational pattern which does not significantly change for the remainder of the packing event. We note that although the bending modulus of DNA may change upon its confinement, the bending properties of DNA play a major role during the first half of the packaging trajectory, i.e., when DNA is not highly confined. Despite the formation of the global structure at this point, the motion of DNA strands relative to each other is quite large; it significantly decreases when more than 75% of genome is packed. The latest stages exhibit the order of DNA on both global and local scales.

Onsager’s classical theory [25] and its extensions developed for semiflexible chains [24] characterize a structural phase transition by introducing an orientational order parameter given by Eq. (2). However, in such systems as bacteriophages the choice of the nematic director is not always obvious. One can use the direction of the X axis, along which the packaging occurs. However, this axis does not always correspond to the predominant alignment of segments of DNA inside bacteriophages (see Fig. 1).

2. Internally defined order parameter

To eliminate an arbitrary selection of the nematic director, we used a more general definition, where the order parameter is calculated as the largest eigenvalue of the second-rank tensor defined by Eq. (4). The global orientational order parameter is shown in Fig. 3(a) as a function of the volume fraction of DNA packed. For both $\phi 29$ and $\epsilon 15$ systems it fluctuates between values 0.6 and 0.8 and does not reveal a significant dependence on packing density. This is because the distribution of the direction of the DNA segments does not change much upon packaging (i.e., roughly the same fraction of the segment vectors points to a particular direction at every value of the packing density). Therefore, this order parameter cannot be used to quantify the ordering inside the capsids.

Because of this, we also calculated the local orientational order parameter [54] using Eq. (3). This describes the preferred direction of a small group of segments around some point inside the capsid. The values of S_{local}^2 are shown in Fig. 3(b). This plot reveals that at low packing densities, which correspond to the initial stages of packing, DNA is highly disordered; a rapid growth in the order parameter is observed in the range of 0.15–0.3, reaching values of 0.8 and 0.85 for $\phi 29$ and $\epsilon 15$, respectively. Since this increase in the order parameter, S_{local}^2 , occurs over a wide range of the DNA con-

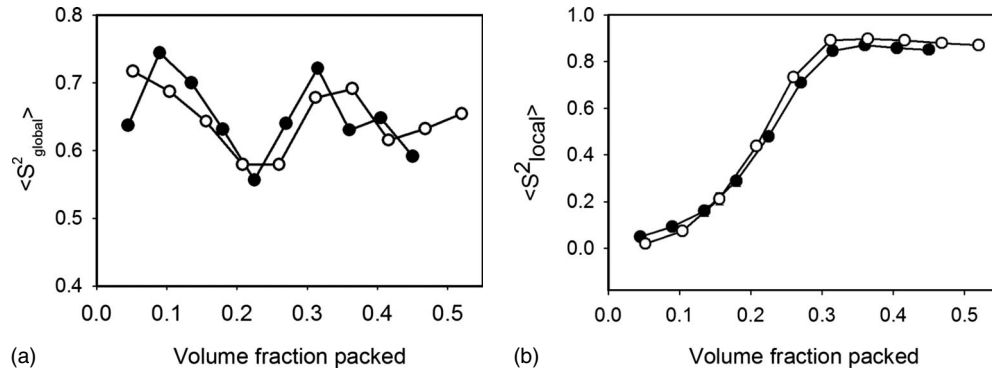


FIG. 3. Values of (a) global and (b) local orientational order parameter that characterizes the transition from isotropic to nematic phase. Data for $\phi 29$ and $\epsilon 15$ are shown by filled and open circles, respectively.

centrations, the observed phenomenon does not represent a classical phase transition but rather a smeared crossover to the nematic phase.

Although the behaviors of both phage systems in Fig. 3(b) are qualitatively similar, the values of the order parameter obtained for $\epsilon 15$ are smaller than those for $\phi 29$ at lower packing densities and larger at higher densities. This is because the dimensions of $\epsilon 15$ capsid are greater than those of $\phi 29$. At lower packing densities, $\epsilon 15$ systems, which are less confined, are more disordered; whereas at the higher densities the additional order appears because a larger fraction of DNA segments is located in the outer layers of spooled structures and have greater radii compared to those of $\phi 29$. The analysis of conformations shows that the degree of DNA organization inside the capsids is inhomogeneous: it is more ordered at the outer layers and more disordered in the inner layers due to increased bending stress in the capsid's interior. This is confirmed by the histogram shown in Fig. 4, which demonstrates the relative number of segments with a given value of the local-order parameters. The coexistence of more ordered domains at the outer layers of the capsids and more disordered domains at the inner space of the capsids is the main reason why the transition observed in Fig. 3(b) is smeared over a wide range of density. Of course, the transition region has an inherent width due to the finite size of the systems studied here. The data obtained for the finite size genomes packed inside the bacteriophage does not represent

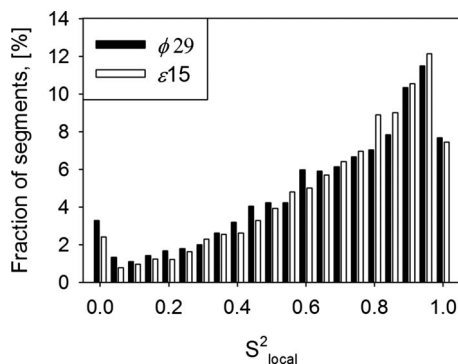


FIG. 4. Distribution of the individual values of the local orientational order parameter, S^2_{local} , (before averaging) for fully packed bacteriophages $\phi 29$ and $\epsilon 15$.

the thermodynamic limit valid for bulk systems, for which the theoretical predictions have been made.

The observed structural inhomogeneity illustrates the interplay between the enthalpic and entropic components of the free energy during packaging. At early packing stages the DNA is free to explore all conformations and the free energy is optimized by minimizing the enthalpy; minimization of the dominating bending energy leads to the formation of distinct structural patterns (e.g., folded toroids and coaxial spools). At later stages, the motion of the DNA is severely restricted due to a high packing density, and the free energy is optimized by not only minimizing the electrostatic interactions but also maximizing the conformational entropy as shown by the disordered inner layers of DNA [41,42].

According to the theoretical predictions of an ensemble of semiflexible chains [24,26], a disorder-order phase transition should occur in a range of the DNA volume fraction of $\sim 0.21-0.22$ ($\sim 11\ell/d$, where $\ell=1000$ Å is the Kuhn's segment length and $d=20$ Å is a diameter of DNA), with the value of the orientational order parameter of 0.49. It has been demonstrated that a renormalization that accounts for the charged nature of the polymer leads to the higher values of the order parameter and lower values of DNA densities, at which the transition occurs [55]. This theory also predicts that the transition to nematic phase should occur in a narrow range of DNA concentrations. Nevertheless, the experimentally measured range of concentrations at which DNA ordering occurs was found to be much wider (13–67 mg/mL) than that theoretically predicted [56]. Our data in Fig. 3(b) show that the crossover to the ordered phase inside bacteriophages occurs at higher densities than those experimentally observed on long unconfined DNA molecules. However, both experiments and simulations showed that the range of densities, over which the transition takes place, is much wider than theoretically predicted. As we mentioned earlier, the widening of the transition range for our systems occurs because the order parameter in Fig. 3(b) is an ensemble average over many different conformations. However, due to the difference in the bending stress, more relaxed outer layers undergo the ordering at smaller values of packing densities compared to inner regions, which experience higher bending stresses. Surprisingly, the inhomogeneity of the ordered phase, which leads to the widening of the transition range, has also been seen in the experiments. This phenomenon was explained by

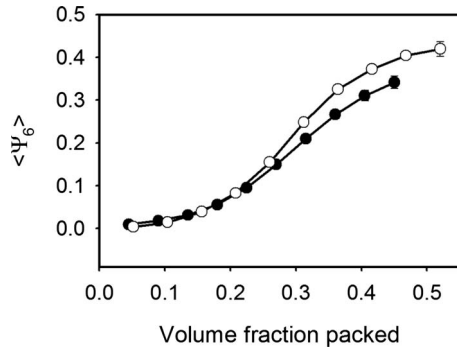


FIG. 5. Bond-orientational order parameter that characterizes the transition from isotropic to hexatic or hexagonal phases. Data for ϕ_{29} and ϵ_{15} are shown by filled and open circles, respectively.

the fact that the very long molecules prevent the appearance of developed microscopically distinct phases due to failure to form well-defined defects between microdomains. Additionally, the observed values of the order parameter are higher than the predicted ones because DNA confined inside the cavity has an additional degree of organization defined by the capsid's geometry. A high degree of ordering in the outer layers may also contribute to this, since the order parameter is averaged over all nearest segments along the chain. We also note that our data correlate well with the recently developed theory of the strong confinement of semiflexible chains [33]. This theory predicts the appearance of structural order in the confined systems at polymer concentrations higher than 0.2. At this point the equations that describe the universal behavior of the confined chains are no longer valid, since the ordering implies the appearance of a specific conformation.

3. Bond-orientational order parameter

In addition to orientation with respect to the director vector and formation of the nematic phase, which is characterized by previously described orientational order parameter, confinement of DNA may also lead to ordering in the plane perpendicular to the nematic director vector. Such ordering results in the appearance of an additional liquid-crystalline hexatic phase. This phase, defined by Toner [57] for the systems of liquid crystals, has also been found for DNA solutions *in vitro* [50]. The appearance of the hexatic phase is described by the bond-orientational order parameter [51–53].

This parameter was calculated according to Eq. (5) for every segment that has nearest neighbors, and the results were averaged over all such segments. The dependencies of this order parameter on packing density are shown in Fig. 5. The bond-orientational order parameter grows significantly in the range of packing densities of 0.2–0.35 reaching values of 0.34 and 0.42 for the fully packed ϕ_{29} and ϵ_{15} , respectively. These values are far below 1, which would be the case for ideal hexatic or hexagonal phases. Comparison of Figs. 3(b) and 5 shows that the sigmoidal crossover of the bond-orientational order parameter occurs in the range of higher densities compared to that of the orientational order parameter. Final values of the bond-orientational order parameter are also lower than the corresponding values of the local

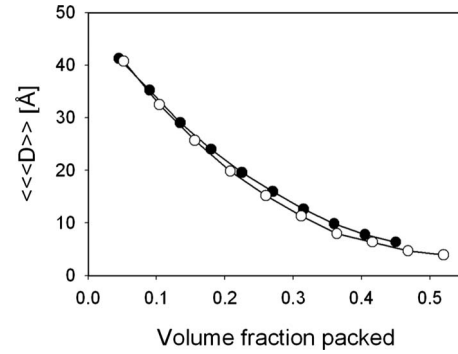


FIG. 6. Average displacement, $\langle D \rangle$, of monomers inside the capsid over 500 ps calculated from the force trajectories vs genome fraction packed. Data for ϕ_{29} and ϵ_{15} are shown by filled and open circles, respectively.

orientational order parameter. All of this leads to the conclusion that fully packed ϕ_{29} and ϵ_{15} even at the local level do not contain a significant amount of the hexatic phase.

B. Characterization of DNA motion

1. Displacement of DNA beads

The visual observation of packaging showed that even when DNA inside the capsids forms a global pattern (at packing densities values ~ 0.2 – 0.25), there is a substantial amount of a local vibrations (undulations) of DNA stands relative to each other. To quantify the amount of motion we plot the average displacement, $\langle D \rangle$, of each bead inside the capsid over 500 ps at zero packing rate (to ensure equilibrium conditions) estimated from the independent MD trajectories (see methods). This is plotted in Fig. 6 and it shows that the average displacement primarily depends on the DNA packing density rather than the DNA conformation or the capsid shape. In the range of packing densities of 0.2–0.3 the displacement of DNA beads inside the capsids is quite substantial (within the range of 10–20 Å). This motion substantially diminishes when the packing density reaches 0.4.

2. Correlation function

The mobility of DNA segments inside the capsids was further analyzed by calculating a correlation function that characterizes an instantaneous orientation of a segment i relative to its initial orientation. These correlation functions calculated by Eq. (6) are shown for different packing densities in Fig. 7. For both bacteriophages ϕ_{29} and ϵ_{15} this function demonstrates that the orientation of the DNA segments calculated for low and intermediate packing densities becomes substantially uncorrelated within several hundreds of nanoseconds as indicated by a drop of this function below the value of 0.5. Contrary, at high packing densities the orientation of DNA segments remains highly correlated, which evidences their limited mobility. These results are consistent with the data shown in Fig. 6, and together they suggest a transition to a more restricted conformational space that can be characterized by a formation of stable domains.

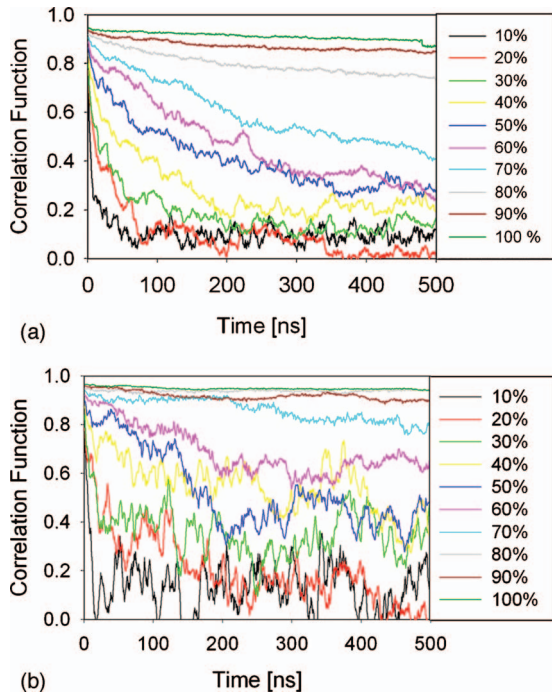


FIG. 7. (Color) The correlation function between the initial and current orientation of DNA segments calculated from 500 ns equilibrium trajectories: (a) $\phi 29$ and (b) $\epsilon 15$.

3. DNA relaxation

To quantify the transition from low to high correlation between states, we calculated the relaxation time by fitting the data of the correlation functions obtained from Eq. (6) into the double-exponential function given by Eq. (7). The fitted slow relaxation times are shown in Fig. 8. Unlike the results seen for the order parameters S_{local}^2 and Ψ_6 , for which a substantial growth was observed in the range of intermediate densities (0.15–0.3), the relaxation times dramatically increase in the range of high packing densities (0.35–0.5). These observations together with our previous data, which showed that the energy of systems during these simulations performed at zero packaging rate remained constant [41], suggest that at low densities the system explores a large number of isoenergetic states and at high densities it is ki-

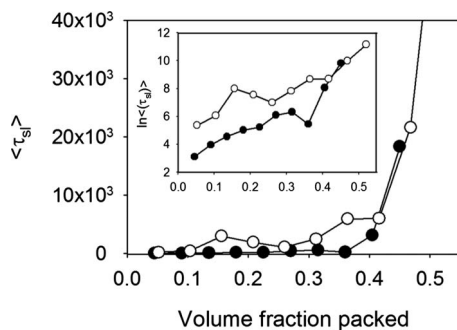


FIG. 8. Correlation time obtained by fitting the correlation functions (Fig. 7) into Eq. (7). Data for $\phi 29$ and $\epsilon 15$ are shown by filled and open circles, respectively. Inset depicts the values of the correlation time on a semilogarithmic plot.

netically trapped in one of many local minima. Thus, at high-densities DNA motion is restricted; conformations turn into a “glassy” state, and form persistent locally ordered domains. It has been proposed [58] that the thin layers of water molecules between DNA strands may lubricate the DNA surface and increase the mobility of tightly packed DNA. The lubrication phenomenon has not been studied in this instance. It is most likely this lubricated motion would be predominately reptation and would not drive changes in the overall DNA topology.

Glassy behavior of DNA inside bacteriophages at high densities has recently been confirmed experimentally [59,60]. In the presence of polycations, partially packed lambda phages reveal the transitions to the toroidal conformations, whereas this transition is not observed for fully packed lambda phages. A similar observation was made for T5 phages [61]. This is direct evidence that DNA is kinetically trapped at the high packing densities. Thus, the formation of a global pattern (folded toroid or coaxial spool) at intermediate densities significantly reduces the number of available conformations, but the motion of DNA on a local scale (DNA undulations) is still significant; further increase in the density results in the crossover to a glassy state, in which motion of DNA is highly restricted. Such a transition has been experimentally observed by measuring the osmotic pressure in systems of hexagonally packed DNA bundles and observing additional pressure at separation distances of 30–35 Å between DNA strands. It has been hypothesized that this happens due to a loss of configurational entropy [62,63]. Our data reveal that, at the range of this transition, the DNA interstrand separation is about 31–34 Å, and, therefore, lend support to this hypothesis.

We also note that in the intermediate range of packing densities the correlation function calculated for $\epsilon 15$ is systematically higher than that for $\phi 29$. This could be due to the presence of the large protein portal inside $\epsilon 15$, which plays an additional organizational role and constrains the mobility of DNA beads. The ordering role of the protein portal has been noticed in our previous publications [13,42]. At high packing densities the correlation functions reach values close to 1, which implies that the motion of DNA inside fully packed bacteriophages is very restricted, which is in agreement with a visual observation of packing trajectories (<http://rumour.biology.gatech.edu/Publications/showcase.html>).

Our thermodynamic analysis has revealed [41,42] that DNA packing inside viral capsids is associated with a significant entropic penalty. While Figs. 3(b) and 7 suggest that the ordering of DNA occurs through two transitions, the entropic contribution to the free energy was found to grow monotonically as a function of the packing density for both $\phi 29$ and $\epsilon 15$ systems. In Fig. 9 we show the dependences of forces pushing DNA outside of the capsid as a function of the genome length packed [41,42]. These results are in good agreement with available experimental data [1,64]. Our previously reported decomposition of free energy [41,42] showed that a significant fraction of a free energy (~35%) is due to entropic penalties. We believe that the cost of confinement significantly dominates the entropic penalty associated with the loss of DNA mobility. The problem of DNA confinement inside a spherical cavity requires further attention of theoreticians and modelers.

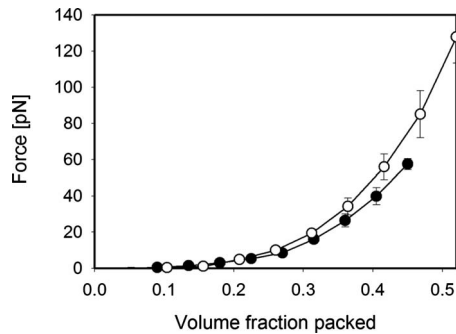


FIG. 9. The force vs volume fraction packed. Data for ϕ_{29} and ϵ_{15} are shown by filled and open circles, respectively.

IV. CONCLUSIONS

We propose a methodology to analyze the conformations of linear polymers confined inside irregular closed cavities over a wide range of packing densities. The analysis of the order parameters revealed that the ordering of DNA to its fully packed structure occurs through two steps: the first step, characterized by the smeared crossover of the order parameter S_{local}^2 , is associated with the formation of the global patterns (folded toroid for ϕ_{29} or coaxial spool for ϵ_{15})

and occurs in the range of packing densities of 0.15–0.3. It represents a smeared transition from isotropic to nematic phases that occurs in different regions of the capsid (inner vs outer) at different densities. At the second step, DNA loses its mobility and becomes kinetically trapped; this happens in the range of volume fraction packed of 0.35–0.5. This corresponds to a dynamic crossover to glassy behavior. Both of these “transitions” can be visually observed by monitoring the packing trajectories. Even though the DNA conformations inside ϕ_{29} and ϵ_{15} are different, we observe that both systems exhibit similar qualitative behavior as the density of DNA increases.

Comparison of the numerical values of the order parameters calculated for ϕ_{29} and ϵ_{15} systems showed that ϵ_{15} is more ordered than ϕ_{29} over the wide range of packing densities. The origin of such additional order must be related to a presence of the large protein portal that penetrates deep inside the capsid of ϵ_{15} . The fully packed ϵ_{15} is more ordered than ϕ_{29} because of higher values of packing density.

ACKNOWLEDGMENT

This research was supported by NIH grant No. GM70785 to S.C.H.

-
- [1] D. E. Smith, S. J. Tans, S. B. Smith *et al.*, *Nature (London)* **413**, 748 (2001).
- [2] J. E. Johnson and W. Chiu, *Curr. Opin. Struct. Biol.* **17**, 237 (2007).
- [3] Y. Xiang, M. C. Morais, A. J. Battisti *et al.*, *EMBO J.* **25**, 5229 (2006).
- [4] W. Jiang, J. Chang, J. Jakana *et al.*, *Nature (London)* **439**, 612 (2006).
- [5] J. Arsuaga, R. K. Z. Tan, M. Vazquez *et al.*, *Biophys. Chem.* **101–102**, 475 (2002).
- [6] D. Marenduzzo and C. Micheletti, *J. Mol. Biol.* **330**, 485 (2003).
- [7] I. Ali, D. Marenduzzo, and J. M. Yeomans, *J. Chem. Phys.* **121**, 8635 (2004).
- [8] I. Ali, D. Marenduzzo, and J. M. Yeomans, *Phys. Rev. Lett.* **96**, 208102 (2006).
- [9] A. J. Spakowitz and Z. G. Wang, *Biophys. J.* **88**, 3912 (2005).
- [10] J. Kindt, S. Tzllil, A. Ben-Shaul *et al.*, *Proc. Natl. Acad. Sci. U.S.A.* **98**, 13671 (2001).
- [11] C. Forrey and M. Muthukumar, *Biophys. J.* **91**, 25 (2006).
- [12] C. R. Locker and S. C. Harvey, *Multiscale Model. Simul.* **5**, 1264 (2006).
- [13] C. R. Locker, S. D. Fuller, and S. C. Harvey, *Biophys. J.* **93**, 2861 (2007).
- [14] J. C. LaMarque, T. V. L. Le, and S. C. Harvey, *Biopolymers* **73**, 348 (2004).
- [15] S. Tzllil, M. Deserno, W. M. Gelbart *et al.*, *Biophys. J.* **86**, 2037 (2004).
- [16] S. Tzllil, J. T. Kindt, W. M. Gelbart *et al.*, *Biophys. J.* **84**, 1616 (2003).
- [17] P. K. Purohit, M. M. Inamdar, P. D. Grayson *et al.*, *Biophys. J.* **88**, 851 (2005).
- [18] P. K. Purohit, J. Kondev, and R. Phillips, *Proc. Natl. Acad. Sci. U.S.A.* **100**, 3173 (2003).
- [19] T. Odijk, *Biophys. J.* **75**, 1223 (1998).
- [20] A. Evilevitch, L. T. Fang, A. M. Yoffe *et al.*, *Biophys. J.* **94**, 1110 (2008).
- [21] I. A. Nyrkova, A. N. Semenov, and J. F. Joanny, *J. Phys. II* **7**, 847 (1997).
- [22] A. Y. Grosberg, *Biofizika* **24**, 32 (1979).
- [23] I. A. Nyrkova, A. N. Semenov, and J. F. Joanny, *J. Phys. II* **7**, 825 (1997).
- [24] A. I. U. Grosberg and A. R. Khokhlov, *Statistical Physics of Macromolecules* (AIP Press, New York, 1994).
- [25] L. Onsager, *Ann. N. Y. Acad. Sci.* **51**, 627 (1949).
- [26] D. V. Kuznetsov, *J. Chem. Phys.* **103**, 7618 (1995).
- [27] E. Casassa, *J. Polym. Sci. [B]* **5**, 773 (1967).
- [28] P. G. de Gennes, *Scaling Concepts in Polymer Physics* (Cornell University Press, Ithaca, N.Y., 1979).
- [29] M. Daoud and P. G. de Gennes, *J. Phys. (France)* **38**, 85 (1977).
- [30] M. Rubinstein and R. H. Colby, *Polymer Physics* (Oxford University Press, Oxford, New York, 2003).
- [31] T. Sakaue and E. Raphael, *Macromolecules* **39**, 2621 (2006).
- [32] S. Jun, A. Arnold, and B. Y. Ha, *Phys. Rev. Lett.* **98**, 128303 (2007).
- [33] T. Sakaue, *Macromolecules* **40**, 5206 (2007).
- [34] R. P. Mondescu and M. Muthukumar, *Phys. Rev. E* **57**, 4411 (1998).
- [35] C. Y. Kong and M. Muthukumar, *J. Chem. Phys.* **120**, 3460 (2004).
- [36] A. Pais, M. G. Miguel, P. Linse *et al.*, *J. Chem. Phys.* **117**,

- 1385 (2002).
- [37] A. Cacciuto and E. Luijten, Phys. Rev. Lett. **96**, 238104 (2006).
- [38] A. Cacciuto and E. Luijten, Nano Lett. **6**, 901 (2006).
- [39] G. Morrison and D. Thirumalai, Phys. Rev. E **79**, 011924 (2009).
- [40] D. Marenduzzo, Math. Comput. Methods Physiol. **9**, 317 (2008).
- [41] A. S. Petrov and S. C. Harvey, Structure **15**, 21 (2007).
- [42] A. S. Petrov, K. Lim-Hing, and S. C. Harvey, Structure **15**, 807 (2007).
- [43] E. Katzav, M. Adda-Bedia, and A. Boudaoud, Proc. Natl. Acad. Sci. U.S.A. **103**, 18900 (2006).
- [44] A. S. Petrov, M. B. Boz, and S. C. Harvey, J. Struct. Biol. **160**, 241 (2007).
- [45] A. S. Petrov and S. C. Harvey, Biophys. J. **95**, 497 (2008).
- [46] H. J. C. Berendsen, J. P. M. Postma, W. F. Vangunsteren *et al.*, J. Chem. Phys. **81**, 3684 (1984).
- [47] R. K.-Z. Tan, A. S. Petrov, and S. C. Harvey, J. Chem. Theory Comput. **2**, 529 (2006).
- [48] R. Eppenga and D. Frenkel, Mol. Phys. **52**, 1303 (1984).
- [49] D. Frenkel and R. Eppenga, Phys. Rev. Lett. **49**, 1089 (1982).
- [50] R. Podgornik, H. H. Strey, K. Gawrisch *et al.*, Proc. Natl. Acad. Sci. U.S.A. **93**, 4261 (1996).
- [51] R. Bruinsma and D. R. Nelson, Phys. Rev. B **23**, 402 (1981).
- [52] B. I. Halperin and D. R. Nelson, Phys. Rev. Lett. **41**, 121 (1978).
- [53] D. R. Nelson and B. I. Halperin, Phys. Rev. B **19**, 2457 (1979).
- [54] R. W. Ruhwandl and E. M. Terentjev, Phys. Rev. E **56**, 5561 (1997).
- [55] G. J. Vroege, J. Chem. Phys. **90**, 4560 (1989).
- [56] K. Merchant and R. L. Rill, Macromolecules **27**, 2365 (1994).
- [57] J. Toner, Phys. Rev. A **27**, 1157 (1983).
- [58] T. Odijk Philos. Trans. R. Soc. London, Ser. A, **362**, 1497 (2004).
- [59] X. Qui, D. C. Rau, V. A. Parsegian *et al.*, Biophys. J. **96**, 422a (2009).
- [60] M. Castelnovo and A. Evilevitch, Eur. Phys. J. E **24**, 9 (2007).
- [61] A. Leforestier and F. Livolant, Proc. Natl. Acad. Sci. U.S.A. **106**, 9157 (2009).
- [62] V. A. Parsegian, R. P. Rand, and D. C. Rau, *Energetics Of Biological Macromolecules*, (Academic Press, San Diego, 1995), Vol. 259, p. 43.
- [63] D. C. Rau and V. A. Parsegian, Biophys. J. **61**, 246 (1992).
- [64] D. N. Fuller, J. P. Rickgauer, P. J. Jardine *et al.*, Proc. Natl. Acad. Sci. U.S.A. **104**, 11245 (2007).